Applied Catalysis B: Environmental 240 (2019) 201–214

Contents lists available at ScienceDirect

Applied Catalysis B: Environmental

journal homepage: www.elsevier.com/locate/apcatb

Efficient heterogeneous electro -Fenton incineration of a contaminant of emergent concern-cotinine- in aqueous medium using the magnetic double perovskite oxide Sr_2FeCuO_6 as a highly stable catalyst: Degradation kinetics and oxidation products

Samia Ben Hammouda[a,*], Claudio Salazar[b], Feiping Zhao[a], Deepika Lakshami Ramasamy[a,b,c], Evgenia Laklova[a], Sidra Iftekhar[a], Indu Babu[a], Mika Sillanpää[a,c,**]

[a] Laboratory of Green Chemistry, School of Engineering Science, Lappeenranta University of Technology, Sammonkatu 12, FI-50130 Mikkeli, Finland
[b] Department of Civil and Environmental Engineering, Florida International University, Miami, FL 33174, USA
[c] Facultad de Ciencias Químicas, Laboratorio de Trazas Elementales y Especiación (LabTres), Universidad de Concepción, 4070371, Edmundo Larenas 129, Concepción, Chile

ARTICLE INFO

Keywords:
perovskite
Fenton
heterogeneous
magnetic
catalysis

ABSTRACT

Cotinine, the majormetabolite of nicotine, has been recently detected in the environment and considered as emerging contaminant in waters. Its chemical treatment has scarcely been investigated in the literature. Here, we show for the first time that double perovskite oxide can be used as heterogeneous catalyst for electrochemical advanced oxidation application and cotinine was selected as the target pollutant. Highly stable magnetic double perovskite Sr_2FeCuO_6 was synthetized for this purpose. The cotinine mineralization in a synthetic sulfate solution of pH 3.0 has been comparatively assessed by anodic oxidation with ($AO-H_2O_2$-BDD) and without electro-generated hydrogen peroxide (AO-BDD) and by the heterogeneous electro-Fenton (EF) processes using the magnetic double perovskite Sr_2FeCuO_6 as the heterogeneous catalyst. The comparative electrolysis experiments were carried out with 500 mL stirred reactor equipped with a boron-doped diamond (BDD) and a carbon felt cathode. Faster mineralization decay was observed with the electro Fenton process due to the additional oxidation by hydroxyl radicals produced from Fenton´s reaction between the iron sites and the electro-generated hydrogen peroxide at the cathode. Moreover, the synergistic effect of the cuprous sites was pointed out. The leaching test confirms the high stability of the catalyst and its heterogeneous action. The influence of current intensity and cotinine concentration was examined. Seven stable organics intermediates were detected and four of them were identified as *N*-Hydroxymethyl norcotinine, norcotinine, 4-oxo-4-(3-pyridyl) butanoic acid and 4-(3-Pyridyl)-3-butenoic Acid. The initial N was released as nitrate and, in smaller proportion, as ammonium ion. Short chain aliphatic acids, mainly oxalic and formic acids were detected. EPR analyses revealed that cotinine was mainly decomposed by the attack of $^{\cdot}OH$. A reaction sequence for cotinine mineralization involving all the detected products is finally proposed. The reusability of the magnetic catalyst for at least 3 times highlights the practical applicability of the envisaged heterogeneous process.

1. Introduction

The presence of nicotine in the aquatic environment is now recognized as an important issue, causing adverse impacts on the ecosystem and human health over the long term [1]. Cotinine [(S)-1-methyl-5-(3-pyridinyl)-2-pyrrolidinone] (Fig. 1a) is the major metabolite of nicotine [2]. Recently, cotinine has been classified as contaminant of emerging concern (CEC) due to its identification in surface-water environments and even in tap waters [3]. Cotinine was the most frequently detected CECs, being found in 95% of fresh leachate from landfills in the conterminous United States (reporting limit range = 63 ng L^{-1}). The high frequency of cotinine detection was also reported

* Corresponding author.
** Corresponding author at: Laboratory of Green Chemistry, School of Engineering Science, Lappeenranta University of Technology, Sammonkatu 12, FI-50130 Mikkeli, Finland.
E-mail addresses: Samia.Ben.Hammouda@lut.fi (S.B. Hammouda), mika.sillanpaa@lut.f (M. Sillanpää).

https://doi.org/10.1016/j.apcatb.2018.09.002
Received 1 May 2018; Received in revised form 5 August 2018; Accepted 1 September 2018
Available online 04 September 2018
0926-3373/

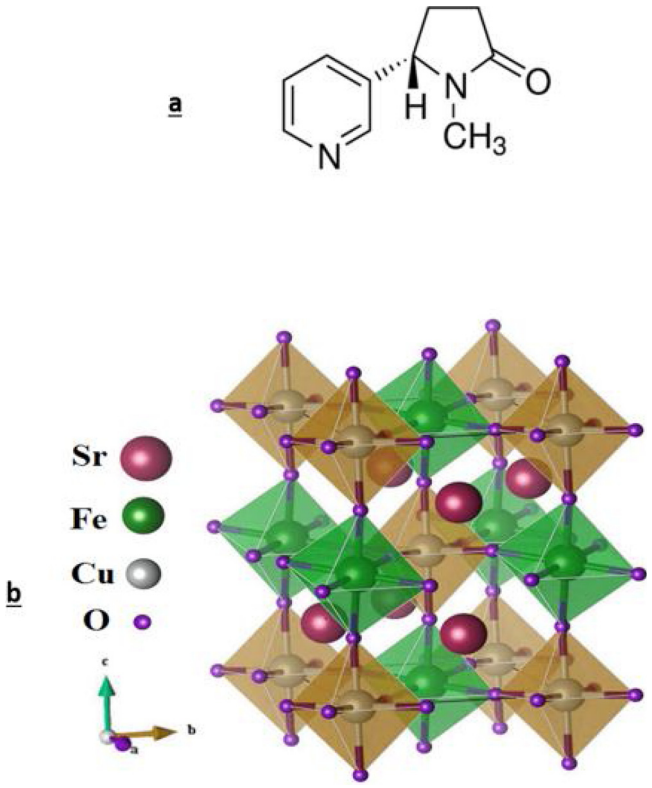

Fig. 1. a-Structure of the generic double Perovskite crystal Sr_2FeCuO_6, b-Molecular structure of cotinine.

in other studies of landfill leachates, as many discarded household/industrial products end up in landfills [4–6]. Cotinine has subtle, enduring developmental consequences. Some cardiovascular effects of nicotine can plausibly arise via conversion into cotinine. Low-level exposure to this metabolite may pose unrecognized perinatal risks [7].

Advanced oxidation processes (AOPs) have proven to be highly efficient for rapid decontamination of recalcitrant and non-biodegradable compounds in water [8]. Among them, electrochemical advanced oxidation processes (EAOPs) have emerged over the last decade as novel attractive techniques for the treatment of a broad-range of organic pollutants that do not require the introduction of reagent due to its generation from redox reactions [9–11]. They are based on the in situ electro-generationof the highly reactive hydroxyl radicals (˙OH), *the second strongest oxidizing agent known*after fluorine with E° (˙OH/OH^-) = 2.80 V/SHE. Their high effectiveness for the decontamination of a large range of refractory compounds with complete mineralization has already been proved [12–14]. One of the most commonly used EAOPs is the anodic oxidation process (AO) in which hydroxyl radicals M(˙OH) are produced by water oxidation and adsorbed at the anode surface (M) as shown in Eq. (1) [15]. Particularly, the boron doped diamond anode (BDD) appears to be the more promising one for the effective electrochemical treatment of organic compounds due to its high overpotential for the Oxygen Evolution Reaction, which allows the generation of high yields of the hydroxyl radicals species BDD (˙OH) adsorbed on its surface [16].

$$\mathbf{M + H_2O \rightarrow M\,(^{\cdot}OH) + H^+ + e^-} \quad (1)$$

The other popular $EAOP_S$ is the electro-Fenton process in which hydroxyl radicals are formed simultaneously from water oxidation at the anode surface (Eq. (1)) as well as in the bulk solution from the electrochemically assisted Fenton reaction (Eq. (2)).The performance of this process is based on the in situ electro-generation of hydrogen peroxide in acidic medium by the continuous two- electron reduction of dissolved oxygen at the cathode surface following Eq. (3) [17,18].

$$\mathbf{Fe^{2+} + H_2O_2 \rightarrow Fe^{3+} + {}^{\cdot}OH + OH^-} \quad (2)$$

$$\mathbf{O_2 + 2H^+ + 2\,e^- \rightarrow H_2O_2} \quad (3)$$

A catalytic amount of iron or another transition metal is sufficient to trigger the process, due to the catalytic electro-regeneration of ferrous ions at the cathode (Eq. (4)).

$$\mathbf{Fe^{3+} + e^- \rightarrow Fe^{2+}} \quad (4)$$

Both of the generated radicals (free and adsorbed ˙OH) can then react with the organic matter to oxidize it until reaching the ultimate oxidation stage, i.e. mineralization.

$$\mathbf{R + {}^{\cdot}OH/M\,(^{\cdot}OH) \rightarrow M + H_2O + mineral\ ions} \quad (5)$$

The classical EF process is typically performed using soluble ferrous salts as catalyst source. Other transitions metals, such as copper, have also been employed to promote the Fenton reaction [19].

The homogeneous EF process suffers from certain common disadvantages *of Fenton´s reaction such as the* catalyst loss through hydroxide *precipitation and the post-treatment discharge requirements* [20,21]. To overcome these limitations, many attempts have been performed for the development of heterogeneous catalysts [22,23].

In this frame, our research group has invested recently great effort in the development of new perovskite based catalysts for water treatment by means of hydroxyl and sulfate radical-*advanced oxidation processes* [24,25]. From these previous studies, it was determined that ABO_3-type perovskites could be usedas anefficient heterogeneouscatalyst for the remediationof *pollutants* in contaminated wastewater and aquatic environments.

Recently, layered double perovskite oxides with the general chemical formula $AA'BB'O_6$ (where A and A' are rare earth or alkaline earth metals, B and B' are d-block transition metals) have attracted a great deal of attention due to their high versatility in structure and properties [26–28]. These oxides are known to exhibit important electronic, magnetic and electrochemical properties [29–31]. Despite the promising results mentioned and the huge number of double perovskites formulations, there have been scarce reports about the application of these materials as catalysts for water treatment processes.

Based on our previous research and the results available in the literature, it seemed interesting to explore new catalytic materials belonging to double perovskites structure $A_2BB'O_6$, containing a combination of Fe with other first row transition metal such as Cu, prepared by the citric acid sol–gel method (also referred to as the citrate sol–gel method). To the best of our knowledge, the cotinine remediation in general and its electrochemical mineralization by anodic and electro Fenton process in particular have never been investigated before. The main goal of this work was to show the ability of these electrochemical methods to destroy cotinine. On the other hand, any attention was paid to the use of perovskite in the EF treatment of organic pollutants.

In this study, we investigated the preparation, characterization and application of the double perovskite $Sr_2FeCuO6$ as a heterogeneous catalyst for the EF process in the presence of the most commonly used electrodes; BDD and carbon felt. To the best of our knowledge, this is the first report on synthesis and application of Sr_2FeCuO_6 double perovskite. The main parameters affecting the mineralization behavior of cotinine were optimized. A systematic study on the identification of cotinine oxidation intermediates was conducted.

2. Materials and methods

2.1. Chemicals

Cotinine and 5, 5-Dimethyl-1-pyrroline-*N*-oxide (DMPO) of analytical grade were provided from Sigma- Aldrich. Carboxylic acids and anhydrous sodium sulfate were of reagent grade from Sigma-Aldrich. Citric acid, strontium, iron and copper nitrates were purchased from

Fig. 2. a-The spongy resin obtained by the citrate complex method before the calcination step, b-The Superparamagnetic behavior of the as prepared perovskite catalyst.

Sigma-Aldrich and used for the perovskite synthesis. Solutions were prepared with ultrapure water from the arium⁻pro ultrapure water system (resistivity 18.2 MΩ cm at 25 °C). All solutions were adjusted to pH 3.0 with diluted solutions of analytical grade sulfuric acid purchased from Sigma-Aldrich.

2.2. Catalysts synthesis

Sr_2FeCuO_6 was synthesized by the sol-gel citrate method. Appropriate amounts of copper nitrate, strontium nitrate and iron nitrate were mixed in deionized water. After stirring continuously for 2 h, the stoichiometric amount of citric acid required to form citrate with all the metals ions was further added to the above solution and followed by an additional heating-stirring step of 12 h over 100 °C to evaporate water. The resultant sol-like solution was then dried for 24 h. The obtained resin was then grinded into fine powders and calcined at 700 °C in air for 5 h to remove organic species (Fig. 2).

Single perovskites: $SrFeO_3$ and $SrCuO_3$ were also prepared for comparison in a way almost identical to that reported in previous studies [25,32]

2.3. Catalyst characterization

The powder (XRD) patterns of the catalysts were recorded on a PANalytical Empyrean diffractometer with Co-K (= 1.7809 Å) radiation source. The generator voltage and tube current used were 40 kV and 40 mA, respectively. Microstructure and morphology of the synthesized materials were carried out using (SEM). The elemental composition of the double perovskite was determined using (EDS). The EDS analysis was performed at several points and averaged to obtain the representative results. Nitrogen adsorption/desorption experiment were used for textural studies with Micromeritics' TriStar II PLUS instrument. All the studied samples were pre-degassed in vacuum at 200 °C for 2 h. Specific surface area were determined using the classical BET model. The study of the surface composition and the electronic states of elements in the valence-band region of the double perovskite oxide were recorded on a ESCALAB 250 X-ray photoelectron spectroscopy (XPS) with Al-K (1486.6 eV) as the X-ray source. Reactive oxygen species (ROS) were detected by electron spin resonance spectroscopy using DMPO as a spin trap agent. The EPR spectra were obtained using a CMS-8400 paramagnetic resonance spectrometer. The operating conditions were as following: magnetic field 336.5 ± 6.0 m T width, power attenuation 10 dB, field modulation 0.100 m T, sweep time 100 s, microwave frequency 9450 MHz. 2.4.

The based perovskite crystallite size was calculated according to the Debye-Sherrer formula which gives a relationship between peak broadening in XRD and particle size, and it was found to be 27 nm:

$$D = \frac{K\lambda}{\beta Cos\theta} \quad (6)$$

Where λ is the wavelength of the radiation, θ is the diffraction angle, K is the Debye-Scherrer constant (0.89) and β is the full width at half maximum (FWHM) of the diffraction peak.

2.4. Electrochemical system

All electrochemical experiments were performed in an undivided reactor containing 500 mL of cotinine solution at initial TOC concentration of 34 mg L^{-1} (TOC_0), with a double jacket in which external water circulated to maintain the solution temperature at 25 °C. The cathode was a carbon felt (5 × 5 cm) purchased from Alfa Aesar. The counter electrode (anode) was a 5 cm^2 (5 cm × 1 cm) BDD thin film on silicon substrate provided by NeoCoat. Electrodes were set up with a gap of 3 cm between the anode and the cathode. A power supply EX752 M Multi-Mode Dual Output PSU was used to provide the electrical current required to operate the electrochemical cell. All experiments were conducted under vigorous stirring with a magnetic bar at 300 rpm to ensure homogenization and the transport of reactants toward/from the electrodes. The solution was saturated with oxygen through the experiment to ensure the electrolytic hydrogen peroxide

production at the cathode following Eq. (3). Similarly to optimal experimental conditions determined by Ozcan et al. [33], the supporting electrolyte (Na_2SO_4 at 0.05 M) was dissolved in the cotinine solutions in order to provide the needed conductivity. In all experiments, the pH was adjusted to 3.0 with sulfuric acid. The heterogeneous electro-Fenton assays were conducted with the based perovskite, which played the role of catalyst. A desired amount of the catalyst was added into the solution before starting the electrolysis.

It should be noted that the size of electrodes is crucial in electrochemical processes. Ideally, for the electro Fenton process, the area of the cathode should be larger than the area of the anode because the anode has a higher electrode potential. In this work, cathode: anode ratio was maintained at 1:5 in order to enhance the electro-regeneration of ferrous sites. The use of larger cathode promote the reduction of Fe^{3+} (Eq. (4)) and minimize the oxidation of Fe^{2+} on the anode (Eq. (7)).

$$\equiv \mathbf{Fe^{2+}} \rightarrow \equiv \mathbf{Fe^{3+}} + \mathbf{e^-} \quad (7)$$

2.5. Analytical procedures

Organic matter content concentration was determined by a global parameter, i.e. the total organic carbon (TOC) content of the solution (mgL^{-1}). Samples were collected during the electrolysis and the non-purgeable organic carbon (NPOC) abatement was measured by using a Shimadzu TOC analyzer. Calibration was achieved with potassium hydrogen phthalate solutions. Generated carboxylic acids (acetic, formic, oxalic, oxamic, malonic and succinic) and inorganic anions (nitrate and nitrite) were monitored by ion chromatography equipped with a conductivity detector using a Shodex IC SI-50 4E (4.0mmI.D × 250 mm). The eluent was 3.2 mM Na_2CO_3 and 1 mM $NaHCO_3$ at a flow rate of 0.7 mL min^{-1}. Ammonium was determined using a Shodex IC YS-50 (4.6mmI.D × 125 mm) and 4 mM methanesulfonic acid as eluant.

The cotinine oxidation intermediates were analyzed by a head space gas chromatography–mass spectrometry (GC–MS) (Agilent-GC 6890 N, MS 5975) with agilent DB-5MS GC column dimensions 30 m, 0.25 mm, 0.25 μm. The inlet temperature was 250 °C in split less mode and the injection volume was 1.0 μL. The oven temperature was programmed at 50 °C for 3 min and it raises at the rate of 5 °C/min to 300 °C held for 2 min. The samples were extracted using a strata C18 column and methanol as the extraction solvent. Before injection, the derivatization of compounds in the extracted samples were performed using N-tert-Butyldimethylsilyl-*N*-methyltrifluoro acetamide at 50 °C for 30 min.

The concentrations of Sr, Cu and Fe in the solutions after reaction were measured by inductively coupled plasma (ICP) using Thermo Scientific ICAP 6000 ICP.

3. Results and discussion

3.1. Catalyst characterization

Fig. 3 shows the powder XRD pattern of the Sr_2FeCuO_6 double perovskite recorded at room temperature. Clearly, the diffractogram shows strong diffraction peaks in the scanning range (20°–80°), indicating high purity and crystallinity of the investigated catalyst. The peaks at 26.25°, 33.06°, 37.35°, 46.34°, 54.03°, 67.75° and 80.06° are indexed as the reflection planes of (110) (111) (200) (202) (220) (312) (400). The diffraction peaks of the pattern were indexed on a monoclinic unit cell with ordered Cu and Fe atoms ((space group = Pbnm) with α = γ = 90°, β = 125°, a = 9.604 Å, b = 5.560 Å, and c = 5.545 Å, respectively). In the ordered Sr_2FeCuO_6 double perovskite the Cu and Fe sites alternate in the lattice. The ideal structure of this double-perovskite can be viewed as a regular arrangement of corner-sharing FeO_6 and CuO_6 octahedra alternating along the three crystal directions. We conclude that the obtained polycrystalline powders are single phase and free of any impurity phases within the resolution of the instrument.

The perovskite crystallite size was calculated according to the Debye-Scherrer equation, and it was found to be 27 nm.

The typical morphology of the double based strontium perovskite is shown in Fig. 2. Before calcination, the spongy structure was clearly observed. The morphology of Sr_2FeCuO_6 was additionallyexamined through SEM, as presented in Fig. 4a. The SEM micrograph reveals a sponge -like structure with high porous morphology. This porous structure would facilitate the transfer of organics as well as provide larger reaction surfaces and more active sites [34]. The spongy catalyst morphology could be ascribed to the generation of a large amount of gaseous products in a very short period of time during the decomposition and combustion of the reacting precursors [35]. Additionally, the presence of iron and copper on the catalyst surface were confirmed by EDS analysis (Fig. 4b). EDS results showed the homogeneous distribution of all the elements in the Sr_2FeCuO_6 synthesized sample. The EDS elementary mapping led to an elemental composition, expressed as atomic percentage, 27.09, 12.07, 11.34, 44,33% for Sr, Cu, Fe and O, respectively. The weak carbon signal observed at 0.2 KeV was ascribed to the deposition of the samples on carbon conductive tape for the SEM measurement.

In Fig. 2, the superparamagnetic behavior of the double ordered perovskite can be obviously noticed. Basically, the B and B´-cation sublattice in a double perovskite oxide $A_2BB'O_6$ with the B/B´ rocksalt ordering can be considered as a simple framework which can be described as a modification of the simple ABO_3 structure with the B positions occupying by the combination of BO_6 and $B'O_6$ octahedra of adequate charge and size [36,37]. In the monoclinic double perovskite Sr_2FeCuO_6, the magnetic Fe and non-magnetic Cu cations respectively are ordered at the B and B' sites in a rock-salt fashion. The layered material can be viewed as ordered rocksalt structures with parallel sheets of atoms where each sheet is made up of monoclinic arrays. The positive superexchange interaction between Cu and Fe cations and their ordering in distinguishable sites should be the responsible for the so-called magneto capacitance, significant for spintronic materials.

The magnetic structure of the Sr_2FeCuO_6 could be attributed to an ordered arrangement of parallel Fe^{3+} ($3d^5$, S = 5/2) magnetic moments, antiferromagnetically coupled with Cu^{2+} ($3d^9$, S = ½) spins. Since Fe^{3+} is in the high-spin state, its d orbitals are split into spin-up and spin-down states. Magnetic interactions could be mediated by itinerant electrons in the π*-bands coming from the t_{2g} orbitals of Cu ions which leads to a geometrical spin frustration.

XPS was used to investigate the chemical state and surface properties of Sr_2FeCuO_6 double-perovskite, and the obtained Sr 3d, Fe 2p, Cu 2p, and O 1 s core-level spectra of Sr_2FeCuO_6 (700 °C) are presented in Fig. 5. All the XPS spectra were firstly corrected by a Shirley-type background subtraction method, and then the background corrected XPS spectra were further fitted with Gaussian function for various chemical states of the elements. Fig. 5 shows that there are two binding energy (BE) peaks at 531.4 and 528.2 eV in the O 1s core-level spectrum. The peak at 528.2 eV could be assigned to the lattice O^{2-} (O_L) and the other peak is probably ascribed to the hydroxyl and carbonate structures (O_H) [38]. The O_L/O_H ratio was calculated to be 9.12. This might be attributed to the alkaline-earth metal (Sr) is segregated towards the surface to form carbonates. Similar phenomenon has been reported in a $SrFeMoO_6$ double-perovskite [39]. The adsorbed hydroxyl and carbonate oxygen on the surface is the very active oxygen and benefit to the oxidation reaction. The Fe 2p core-level XPS spectrum of Sr_2FeCuO_6 (700 °C) shows a spin-orbit splitting which involves a doublet of $2p_{3/2}$ and $2p_{1/2}$ excitation. The BE peaks at 710.3 and 723.6 eV are the characteristic peaks of $2p_{3/2}$ and $2p_{1/2}$ of Fe^{3+}, respectively. The satellite peak at around 718.9 eV could be assigned to Fe^{3+} species [38], which is in a good agreement with our previous $LaFeO_3$ perovskite. All these findings indicate that the chemical valance state of iron atoms in Sr_2FeCuO_6 perovskite is +3. In the Cu 2p core-

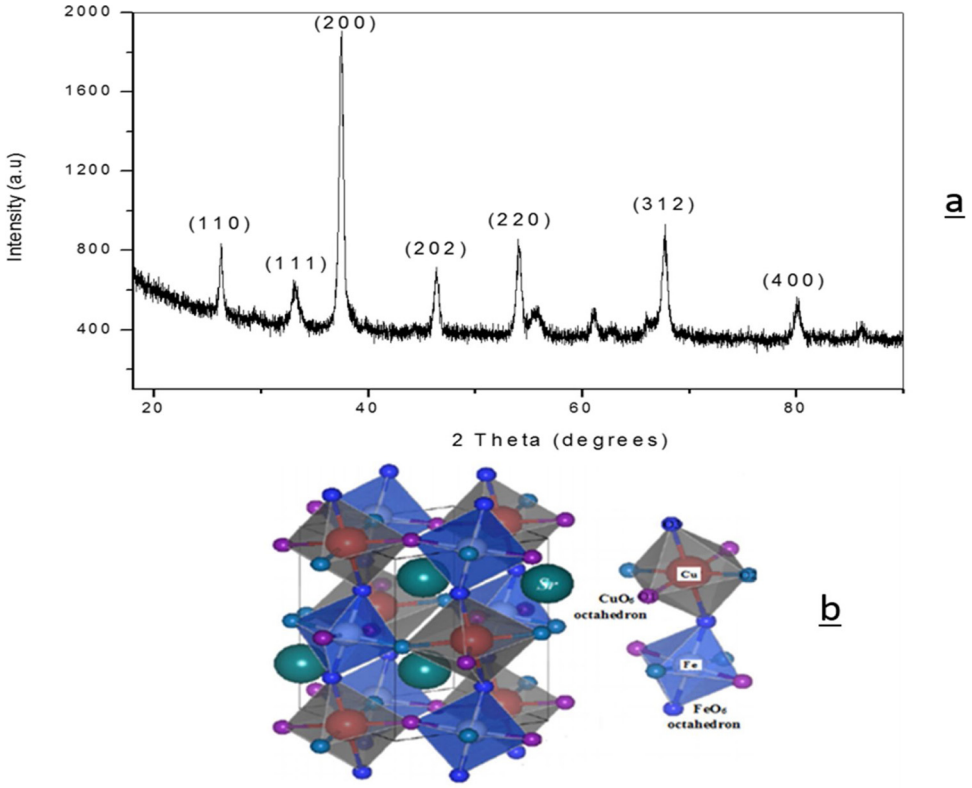

Fig. 3. a- X-ray diffraction patterns of Sr_2FeCuO_6 double perovskite, space: Pbnm; crystal structure: monoclinic with $\alpha = \gamma = 90^{\circ}$, $\beta = 125^{\circ}$, a = 9.604 Å, b = 5.560 Å, and c = 5.545 Å, b- schematic crystallographic representation of the ordered monoclinic double perovskite structure.

level XPS spectrum of Sr_2FeCuO_6 (700 °C), the characteristic peaks of Cu^{2+} were found at 933.9 eV for $2p_{3/2}$ and at 953.6 eV for $2p_{1/2}$. Their shake-up contribution appeared at 943.2 and 962.2 eV, respectively. No obvious peaks of Cu^{+} species were detected in the Sr_2FeCuO_6 (700 °C) by XPS observations. From the intensities of Fe $2p_{3/2}$ and Cu $2p_{3/2}$ peaks, the Fe/Cu atomic ratio in Sr_2FeCuO_6 (700 °C) was calculated to be 0.86 by the method given by [40]. The Fe/Cu ratio is slightly less than the stoichiometric Fe/Cu = 1. In the Sr 3d core-level spectrum two peaks at binding energies of 133.2 and 134.9 eV could be assigned to La $3d_{5/2}$ and $3d_{3/2}$ respectively. Moreover, the BE difference between the peaks of Sr $3d_{5/2}$ and $3d_{3/2}$, which equals to the 3rd layer electronic spin-orbit splitting, is 1.7 eV. All these are in a good agreement with the values observed in the reported single-perovskite $SrCoO_3$ [25] and double-perovskite $SrFeMoO_3$ [39].

The XPS characterization of the used Sr_2FeCuO_6 (700 °C) perovskite has also been conducted and compared with that of the fresh Sr_2FeCuO_6 (700 °C) perovskite. The obtained core-level spectra of each elements are shown in Fig. 6. The significant change was not observed in the used catalyst for Sr 3d, Fe 2p, and Cu 2p, while the peak of OH increased obviously after pollutant treatment. This result is not surprising and it could be attributed to the oxidation of the organic pollutants on the active sites of the catalyst, leading to an increase in the oxygen content on the catalyst surface after reaction. The results reveal the stability of Sr_2FeCuO_6 during the oxidation process.

In order to determine its metals contents, 0.1 g of the perovskite oxide Sr_2FeCuO_6 was dissolved in concentrated sulfuric acid. The metal cations were released and their concentrations were determined by inductively coupled plasma (ICP) using Thermo Scientific ICAP 6000 ICP. The results are illustrated in Table S1.

The nitrogen adsorption/desorption measurements were also carried out to determine the specific surface area and characteristics porosity of Sr_2FeCuO_6 as summarized in Table S2. The BET surface area of Sr_2FeCoO_6 was found to be 4.67 $m^2\ g^{-1}$, with corresponding volume of 0.005 $cm^3\ g^{-1}$.

4. Comparative mineralization behavior of cotinine by EAOPs

Considering the possibility of adsorption phenomena contribution, the capacity and ability of the double perovskite material to adsorb cotinine was firstly assessed in the absence of an electric field. The result depicted in Fig. 7 reveals that after 8 h of contact time with the perovskite nanoparticles, the cotinine TOC decay was not significant. Cotinine was hardly adsorbed on the catalyst surface and just around 4% was removed after a long residence time, showing the weak adsorption affinity between cotinine and the investigated double perovskite oxide. This result is in good agreement with the obtained low specific surface area of Sr_2FeCuO_6(3.705 m^2/g).

The chemical stability test of cotinine at pH 3 [in the absence of H_2O_2 and the catalyst] has also been performed. Change in the concentration has not been observed over the time suggesting that cotinine is highly stable under acidic environment.

Subsequently, the oxidative power of the heterogeneous EF, anodic oxidation (AO) and anodic oxidation in the presence of the electro-generated H_2O_2 (AO-H_2O_2) methods was comparatively ascertained by assessing the mineralization of 500 mL of a 50 $mg\,L^{-1}$ cotinine solutions (equivalent to 34 $mg\,L^{-1}$ TOC) electrolyzed in the BDD/carbon felt cell at pH 3.0, 8 mA cm^{-2} for 480 min, with addition of 0.2 $g\,L^{-1}$ catalyst for the EF process.

As can be seen in Fig. 7, all cotinine solutions tested for the different electrochemical techniques underwent a progressive decay with increasing electrolysis time. No total mineralization was achieved for both AO methods after 8 h of treatment, TOC was reduced by 65% for simple AO, a value slightly lower than the 69% attained in the presence of the electro-generated hydrogen peroxide. The oxidative ability of these treatments is ascribed to the oxidative capacity of BDD ($^{\cdot}OH$) formed from water discharge at the anode surface via Eq. (1), which is the main oxidizing agent in both cases, to destroy cotinine and its oxidation products.

Under similar conditions, faster TOC decay was achieved for the heterogeneous EF than the AO and AO-H_2O_2, up to yield almost

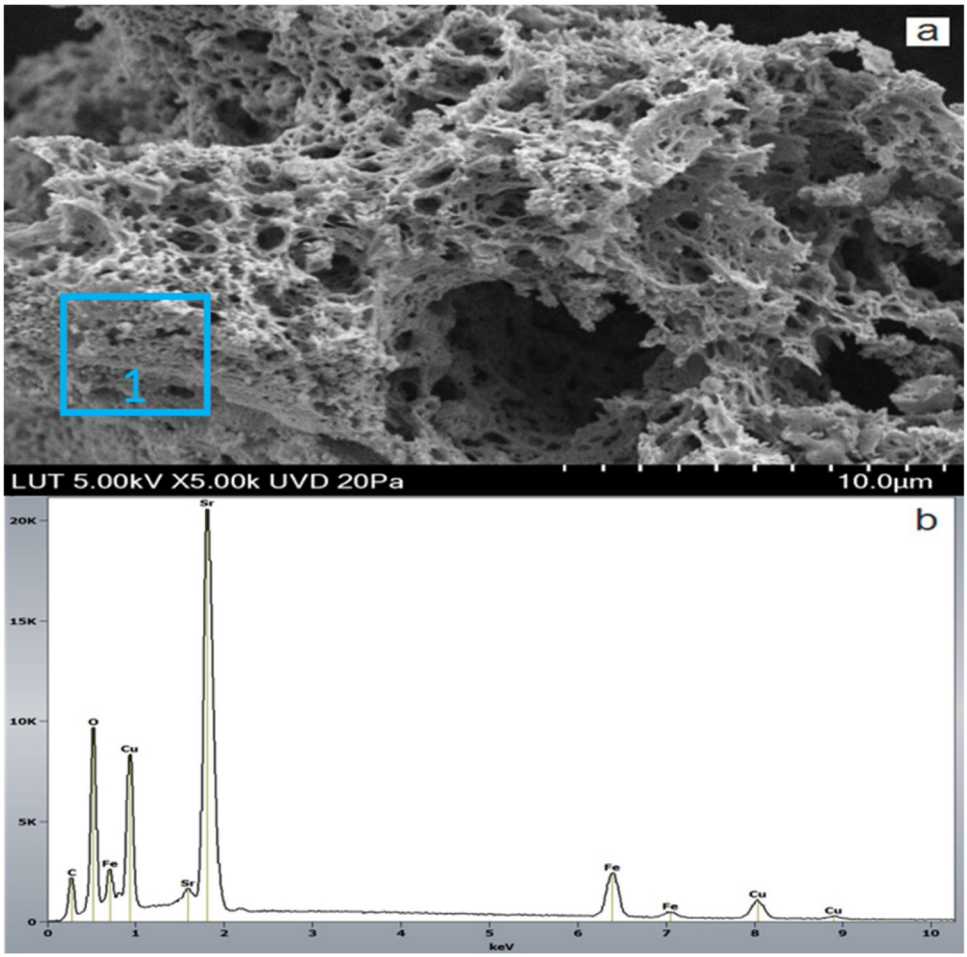

Fig. 4. a- SEM micrograph of the synthesized Sr_2FeCuO_6, b-Energy dispersive X-ray spectroscopy (EDS) spectra acquired in scanning electron microscopy (SEM) at the top view sample of Sr_2FeCuO_6, Acc voltage 15Kv, Scale bars are 5 µm. The blue square labeled 1 in the SEM micrograph marks the location of EDS analysis. (For interpretation of the references to colour in this figure legend, the reader is referred to the web version of this article).

complete mineralization after 8 h of treatment (~93%). The solution TOC was rapidly reduced by 58% during the first 3 h, decreasing much more slowly at longer time to almost 75% after 6 h. The lowest mineralization abatement was achieved for AO which indicates that cotinine and its intermediates react slowly with the physisorbed hydroxyl radicals BDD (**˙OH**) limited by their mass transfer to the anode. In EF, the increase in the cotinine mineralization rate owes to the additional oxidative action of large amounts of ˙OH produced from the catalytic action of the Fenton´s reaction between the electrogenerated H_2O_2 and both ferrous and cuprous active sites on the catalyst surface (Eqs. (8) and (9)).

$$\equiv Fe^{2+} + H_2O_2 \rightarrow \equiv Fe^{3+} + {}^{\cdot}OH + OH^- \quad (8)$$

$$\equiv Cu^{+} + H_2O_2 \rightarrow \equiv Cu^{2+} + {}^{\cdot}OH + OH^- \quad (9)$$

Obviously, we noticed that for the three applied EAOPs processes the rate in TOC decay gradually decreases at longer electrolysis time, probably due to the formation of persistent intermediates which are hardly oxidizable by the generated hydroxyl radicals, as will be better discussed subsequently.

It is worth mentioning that the comparative studies between the catalytic performances of the double perovskite oxide Sr_2FeCuO_6 and the single based perovskites $SrFeO_3$ and $SrCuO_3$ have shown the synergistic effect of Fe^{2+}/Fe^{3+} and Cu^{2+}/Cu^{+} ions in the EF process (Fig. 8a)).

Moreover, possible release of the reactive cupric and ferrous ions in the reaction medium was checked. For the double based perovskite oxide, the leached extent of both transition metals was below the ICP detection limit ($< 0.001\ mg\ L^{-1}$). This finding exclude the possible contribution of homogeneous Fe and Cu in the Fenton reaction and confirms the well-known high stability of double perovskite oxides. Comparison of photoelectron spectra of Sr3d, Fe2p and Cu2p acquired with the fresh and spent catalyst (Fig. 6) leads us to confirm the high stability deducted from the ICP results. Similarly, the single perovskites have shown good stability and only a strontium amount of $0.123\ mg\ L^{-1}$ was detected in the aqueous medium after 8 h of treatment.

For the electro-Fenton system, it is generally assumed that hydroxyl radicals can be produced by the reaction between hydrogen peroxide and the transition metal in acidic medium. In our work, the generation of ˙OH was verifiedby DMPO trappedEPR after reaction 120 min, as depicted in Fig. 8b. The EPR spectrum exhibited a 4-fold characteristic peak of the typical ˙OH/DMPO complex adduct with an intensity ratio of 1:2:2:1 [41].

Under the same applied conditions, the peak intensity of ˙OH/DMPO adduct in the case of Sr_2CuFeO_6 was higher than that of $SrFeO_3$ and $SrCuO_3$, demonstrating that the coexistence of two transition metals enhance the hydrogen peroxide decomposition and therefore the ˙OH production.

4.1. Possible catalytic oxidation mechanism of the heterogeneous electro-Fenton process

The heterogeneous electro-Fenton reaction is a surface-controlled

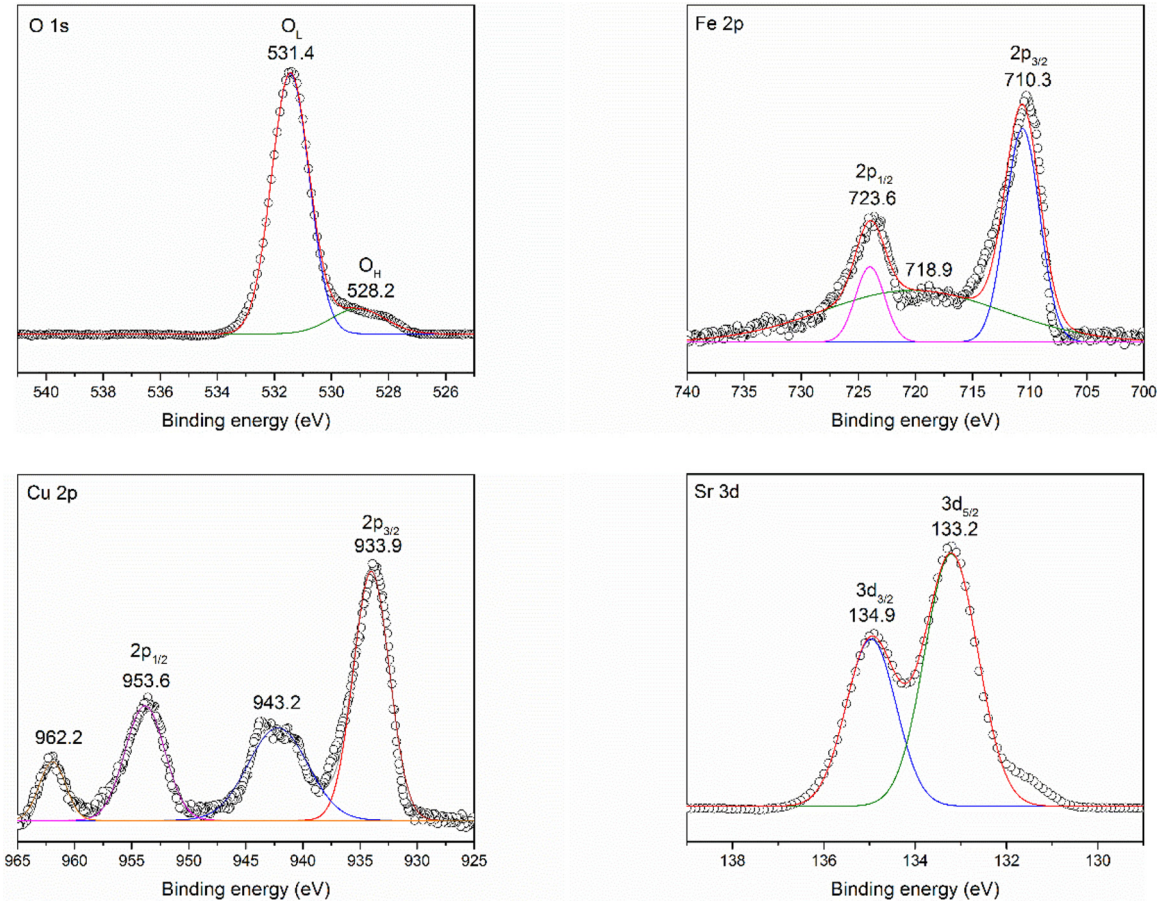

Fig. 5. XPS spectra of Sr 3d, Fe 2p, Cu 2p, and O 1s in the Sr_2FeCuO_6 (700 °C) double-perovskite at room temperature.

system controlled chiefly by the hydrogen peroxide concentration and the catalyst properties. Up to now, its reaction mechanism was not widely agreed upon. Nevertheless, it is largely agreed that the generation of reactive oxygen species from the decomposition of hydrogen peroxide catalyzed by the active sites on the catalyst surface is the most crucial step in the entire EF oxidation process, which fits the Harber-Weiss circle mechanism similarly to the mechanism of the classical homogeneous electro-Fenton reaction [42].

In the initial step of our envisaged EF process, the electrochemically generated hydrogen peroxide adsorbed on the Sr_2FeCuO_6 catalyst would oxidize the Fe^{2+} to Fe^{3+} via a one electron transfer (Eq. (8)) to produce $^{\cdot}OH$ radicals. The presence of the cupric ion sites as co-catalyst on the catalyst surface promotes a quickest mineralization efficiency which is ascribed to the contribution of the Cu^{2+}/Cu^{+} couple to $^{\cdot}OH$ generation and the synergetic effect in the trimettalic (Fe-Cu-Sr) perovskite catalyst. It must be pointed out that, throughout the EF process, the in situ air sparging in addition to the mechanical agitation of the solution allowed the contact of the nanoparticles on the cathode surface. During this contact, copper and iron entities present on the perovskite surface can be reduced. The Cu^{2+} should be reduced to Cu^{+} at the carbon felt surface from reaction (Eq. (11)). Thereafter, hydroxyl radicals can be generated via reaction (Eq. (9)). Furthermore, due to the potential difference between the redox couples Fe^{3+}/Fe^{2+} and Cu^{2+}/Cu^{+}, Cu^{+} can contribute to the regeneration of Fe^{2+} via reaction (Eq. (12)), thus giving rise to additional hydroxyl radicals during the electro-Fenton process. This process would improve the interfacial electron transfer in redox cycles of Fe^{3+}/Fe^{2+} and Cu^{2+}/Cu^{+} pair existed in Sr_2FeCuO_6. On this basis, more $^{\cdot}OH$ radicals can be formed, which enhances the mineralization efficiency during the electro-Fenton catalytic reaction. A schematic of the key steps involved in the heterogeneous Sr_2FeCuO_6 –BDD EF process is presented in Fig. 9.

$$\equiv \mathbf{Fe^{3+}} + \mathbf{H_2O_2} \rightarrow \equiv \mathbf{Fe^{2+}} + \mathbf{HO_2^{\cdot}} + \mathbf{H^{+}} \quad (10)$$

$$\equiv \mathbf{Cu^{2+}} + \mathbf{e^{-}} \rightarrow \equiv \mathbf{Cu^{+}} \quad (11)$$

$$\equiv \mathbf{Cu^{+}} + \equiv \mathbf{Fe^{3+}} \rightarrow \equiv \mathbf{Cu^{2+}} + \equiv \mathbf{Fe^{2+}} \quad (12)$$

As can be seen from Fig. 7b and the good square regression coefficients (R^2), the exponential TOC decay for all the curves of Fig. 7a was well fitted to a pseudo-first-order kinetic model by plotting ln (TOC_0/TOC) vs. time, where TOC_0 and TOC represent the solution TOC at initial time (before electrolysis) and time t, respectively. The corresponding rate constants (k) of EF, AO-H_2O_2 and AO were 0.00397, 0.00213 and 0.00182 min^{-1}, respectively (Fig. 7b). This behavior presupposes the generation of a steady amount of BDD ($^{\cdot}OH$) and/or $^{\cdot}OH$ which are available to attack the organics during all the envisaged electrochemical processes. As can be concluded, the k value is quite similair in AO-BDD and AO-BDD-H_2O_2 and approximately 2-fold lower than that in H-EF-BDD process, confirming that in the two former EAOPS, cotinine is slowly oxidized by the adsorbed BDD (•OH) and much more quickly by the free radicals $^{\cdot}OH$.

The mineralization of organic N–compounds by EAOPS occurs alongside the release of inorganic ions (ammonia, nitrate and nitrite). For the EAOPS tested in this work, the mineralization of cotinine was accompanied by the formation of NO_3^{-} and NH_4^{+}, which were analyzed by ionic chromatography, without detecting the presence of other inorganic nitrogen such as NO_2^{-}. From the comparison of Fig. 10a–c, one can infer that for both treatments NO_3^{-} ion was preferentially generated in relation to NH_4^{+} ion. As can be seen from Fig. 10, the major part of both ions was released during the first 240 min, and at 480 of electrolysis, the solution treated by AO contained 0.41 mM of

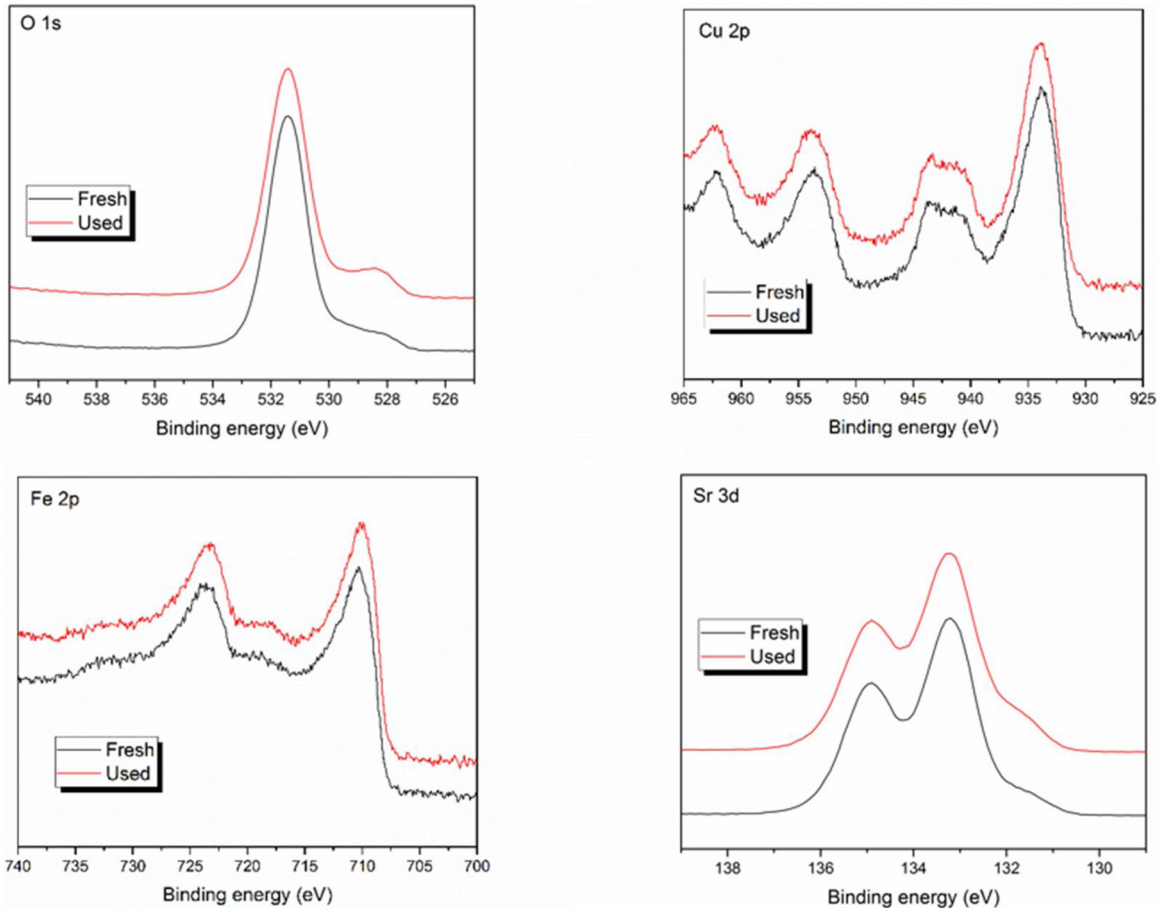

Fig. 6. XPS spectra of Sr 3d, Fe 2p, Cu 2p, and O1s in the Sr_2FeCuO_6 (700 °C) double-perovskite before and after pollutant treatment.

NO_3^- (84% of the initial N (0.57 mM) and 0.053 mM of NH_4^+, whereas that degraded by EF contained 0.48 mM of NO_3^- and 0.062 mM of NH_4^+. The loss of 95% of initial nitrogen as ammonium and nitrate when the solution was almost completely mineralized with 93% TOC decay evidences that almost all initial nitrogen was converted without significant release of organic N-compounds. On the other side, the fact that only 79 and 81% of initial N is converted into NH_4^+ and NO_3^- ions in the anodic systems AO and AO-H_2O_2, respectively, suggests that about 10% of the initial N content remains in the solution as recalcitrant N-derivatives. Also we can suggest that the missing N in the mass balance may be accounted to the formation of volatile N-Species such as N_2 and NO_x as recently demonstrated by Baltruschat research group [43] by differential electrochemical mass spectroscopy.

Based on the aforementioned findings, the theoretical mineralization reaction of cotinine, can be written as reaction (Eq. (13)), with formation of CO_2 and NO_3^- and the consumption of 60 electrons (n):

$$\mathbf{C_{10}H_{12}N_2O + 25\ H_2O \rightarrow 10\ CO_2 + 2NO_3^- + 62H^+ + 60\ e^-} \quad (13)$$

The mineralization current efficiency (MCE) for each trial at applied current I (= 0.200 A) and given electrolysis time t (in h) was then estimated from Eq. (14) [44]:

$$\mathbf{MCE}\ (\%) = \frac{\boldsymbol{\Delta(TOC)nFVs}}{4.23 \times 10^7 \boldsymbol{m\,I\,t}} \times 100 \quad (14)$$

Where, Δ(TOC) shows the amount of TOC removal (mg carbon L^{-1}) at a given time, m is the number of carbon atoms of cotinine molecule (10), F is Faraday constant (96,487 C mol^{-1}) and 4.32×10^7 is the conversion factor of homogenization of units (=3600 sh^{-1} × 12,000 mg mol^{-1}), V_s is the solution volume (L), I is the applied current (A) and t is the electrolysis time in hour (h). n is the number of electrons exchanged per mole of cotinine, which is determined as 60 according to Eq. (13).

Fig. 11a depicts the MCE values calculated from Eq. (14) for the assays shown in Fig. 7. In both AO cases, the current efficiency for BDD fluctuates between 29% and near 10% at 60–480 min of electrolysis, being slightly higher when the EF process was applied [31%-13%]. This means that organic pollutants were mineralized during each run, independently of the main oxidizing species, which was BDD (˙OH) in the former processes and its combination with free (˙OH) in the second one.

The MCE tended to decrease with the course of electrolysis, which can be explained not only by the formation of more resistant intermediates but also by the gradual disappearance of organic matter and the limitations related to low organic loads. For the EF-BDD, AO-BDD-H_2O_2 and AO-BDD processes. The MCE values decayed dramatically from 54, 50 and 46% after 30 min of treatment to 13, 10 and 9% at 480 min.

It is worthy to conclude that high mineralization degrees were obtained during the first 3 h of electrolysis. At this period of time, the mineralization current efficiency was at most favorable levels. These findings suggest that the EF/perovskite process could be integrated in sequential processes with conventional techniques, mainly biological, for industrial applications

For practical applications, energetic parameters are also fundamental figures-of-merit to assess the viability of the applied electrochemical processes. Operating at constant I, the energy consumption per unit volume (EC) and unit TOC mass (EC_{TOC}) are obtained from Eqs. (15) and (16), respectively [9]:

$$\boldsymbol{EC\,(kWhm^{-3})} = \frac{\boldsymbol{E_{Cell}\ I\ t}}{\boldsymbol{Vs}} \quad (15)$$

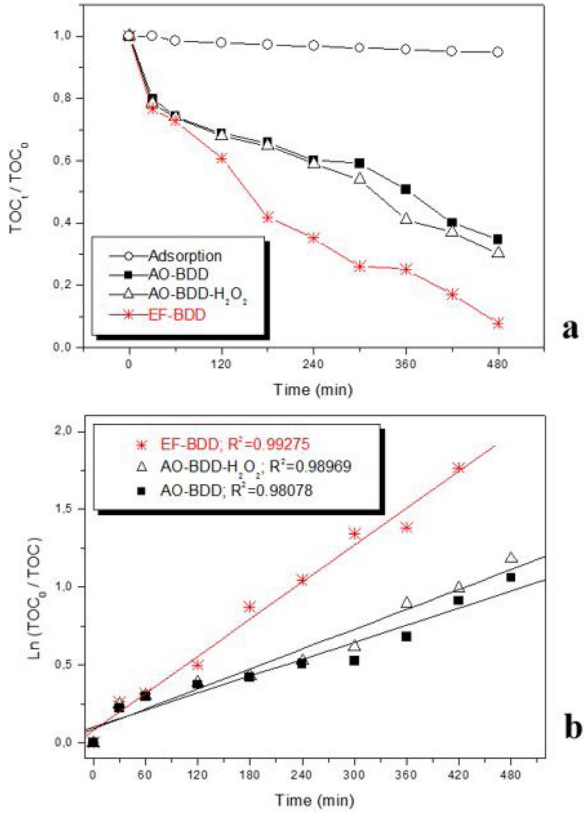

Fig. 7. Cotinine adsorptive behavior (Experimental conditions: no electrode polarization, catalyst = 0.2 g L^{-1}, pH = 3, [cotinine]$_0$ = 50 mg L^{-1} (equivalent to 34 mg L^{-1} TOC), working volume = 500 mL), and its mineralization behavior under AO, AO-H_2O_2 and EF processes using BDD anode (Experimental conditions: [Na_2SO_4] = 0.05 M, pH = 3.0, j = 8 mA.cm^{-2}, working volume of 500 mL, 0.2 g L^{-1} catalyst for the EF process, [cotinine]$_0$ = 50 mg L^{-1}.

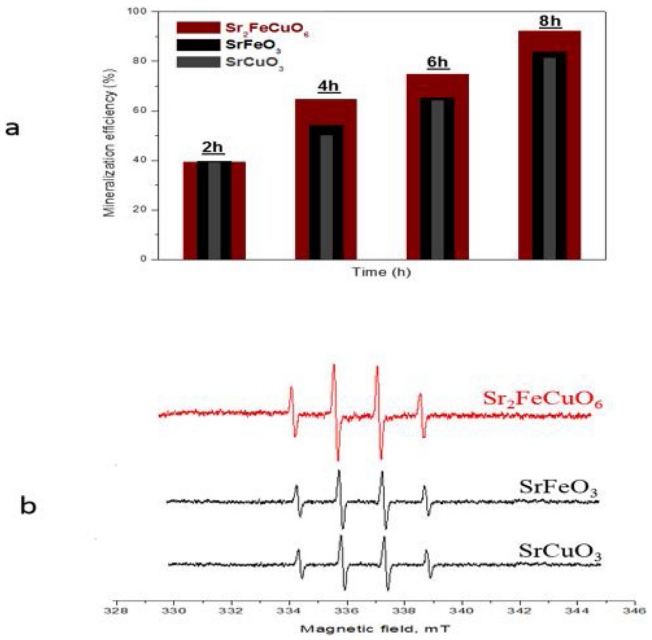

Fig. 8. a- Mineralization of cotinine by the EF process over the double and single based perovskite oxides. b- DMPO spin trapping spectra recorded at pH 3 in aqueous dispersion with Sr_2CuFeO_6, $SrFeO_3$ and $SrCuO_3$, respectively.

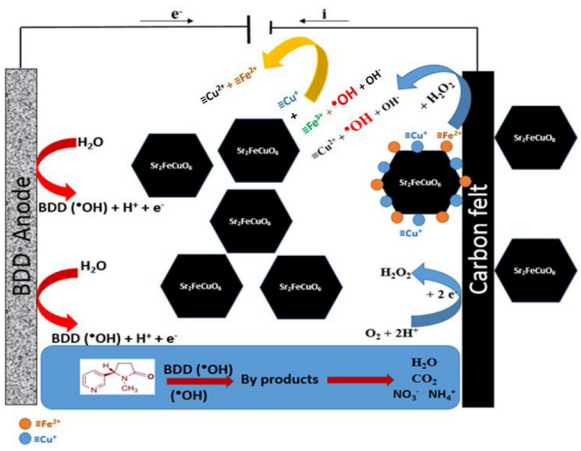

Fig. 9. Schematic presentation of the main steps involved in the electrochemical mineralization of cotinine by the heterogeneous perovskite-BDD Electro Fenton process.

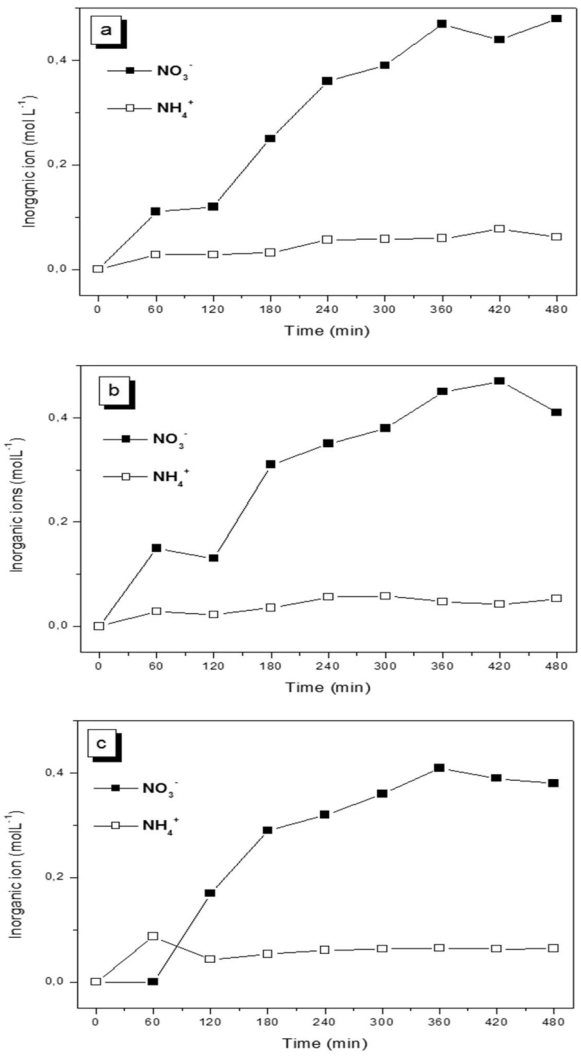

Fig. 10. Time course of inorganic ions: ammonium and nitrate released during the (a) - EF-BDD, (b)- AO-BDD-H_2O_2 and (C)- AO-BDD treatment of 500 mL of 50 mg L^{-1} cotinine solutions under the conditions of Fig. 7.

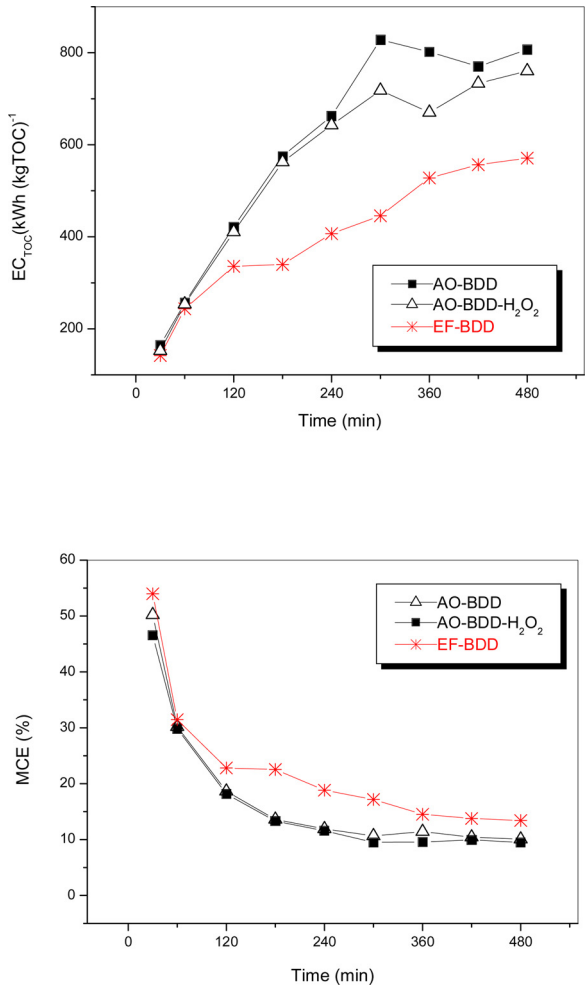

Fig. 11. (a) Mineralization current efficiency with electrolysis, (b) Energy consumption per unit TOC mass with electrolysis time for the AO-BDD, AO-BDD-H_2O_2 and EF-BDD treatment of 500 mL of 50 mg L^{-1} cotinine solutions under the conditions of Fig. 7.

$$EC_{TOC}(kWhg^{-1}TOC) = \frac{E_{Cell}\, I\, t}{(\triangle TOC)Vs} \quad (16)$$

Where E_{cell} is the average potential difference of the cell (V), I is the applied current (A), t is the electrolysis time (h), $\Delta(TOC)_{exp}$ is the experimental TOC decay (mgL^{-1}) and V_s is the volume of the treated solution (L).

The EC_{TOC} calculated for the three processes of Figure according to Eq. (16) is shown in Fig. 11. After 8 h, higher consumptions of about 0.807 and 0.760 KWh (gTOC)$^{-1}$ were required in AO and AO-H_2O_2 respectively, as expected from their much lower mineralization ability than the EF treatment, which required 0.571 KWh (gTOC)$^{-1}$ (18.24 kWhm^{-3}). Considering the value of the industrial KWh in Finland (0.059 EUR per kWh) the energy cost for the overall mineralization of cotinine solutions by EF is 1.076 euro per m^3.

4.2. Effect of the applied current density

The applied current is a key factor in EAOPS because it regulates the amounts of hydroxyl radicals acting as oxidizing agents. The possible impact of this factor upon the mineralization was examined by electrolyzing the above 50 mgL^{-1} cotinine solution of pH 3 for each treatment at 200, 300, 400 and 500 mA for 3 h. Table 1 summarizes the percentage of TOC decay obtained after 1 h and 3 h electrolysis of each trial. In all cases, as expected, faster mineralization was always observed when the current intensity increases, indicating an enhancement of the degradation power of all the investigated electrolytic systems. In the case of AO-H_2O_2, slightly higher TOC decay was achieved, indicating that adsorbed $^{\cdot}OH$ is the major oxidizing species. The enhancement in the mineralization efficiency with increasing the current under electro-Fenton system could be related to the higher generation of free $^{\cdot}OH$ in the medium from Eqs. (8) and (9), due to the fatser cathodic generation of hydrogen peroxide.

The dosage of the electro-generated hydrogen peroxide in the undivided electrolytic cell at different applied current values has been also performed. Hydrogen peroxide concentrations were estimated using the iodometric titration method with $Na_2S_2O_3$ solution. As illustrated in table S3, the highest accumulation of hydrogen peroxide is obtained at 500 mA.

Table 1 reveals that EF-BDD is more efficient than the anodic methods. Fig. 12 shows that the productivity of $^{\cdot}OH$ produced at 400 mA is three times higher than that obtained at 100 mA, indicating that the increase of the current intensity enhances the generation of $^{\cdot}OH$.

For the EF system, the mineralization removal was 58, 62, 69 and 73% after 180 min of electrolysis at 200, 300, 400 and 500 mA, respectively. It should be noted that the mineralization decay is not linearly dependent on the applied current. This behavior could be ascribed to the parallel parasitic reactions. These side reactions involve primordially the oxidation of BDD ($^{\cdot}OH$) to O_2 (Eq. (17)) at the anode and its dimerization to H_2O_2 (Eq. (18)). The dimerization of $^{\cdot}OH$ to H_2O_2 in

Table 1
Percentage of TOC removal mineralization current efficiency (MCE) for the treatment of 500 mL of solution containing 34 mg L^{-1} TOC of cotinine in 0.05 mol L^{-1} Na_2SO_4 at pH 3.0 by several EAOPS at different current intensity.

		After 1 h of treatment			After 3 h of treatment		
Method	Current intensity (mA)	TOC removal (%)	MCE (%)	EC_{TOC} KWh	TOC removal en (%)	MCE (%)	EC_{TOC} KWh
AO-BDD	200	25.27	29.86	0.256	34.35	13.31	0.587
	300	29.31	18.93	0.452	37.32	8.04	1.064
	400	30.68	14.86	0.713	42.35	6.84	1.550
	500	33.01	12.79	1.025	47.98	6.20	2.115
AO-H_2O_2-BDD	200	25.17	30,2	0.247	35.14	13.62	0.562
	300	28.12	18,16	0.471	39.09	8.42	1.016
	400	29.97	14.52	0.730	45.14	7.29	1.454
	500	31.25	13.83	1.054	48.79	6.30	2.079
EF-BDD	200	27.05	31.45	0.243	58.14	22.53	0.339
	300	25.67	16.64	0.516	62.03	13.36	0.640
	400	27.05	13.10	0.809	64.14	10.36	1.023
	500	31.38	12.16	1.078	73.09	9.44	1.388

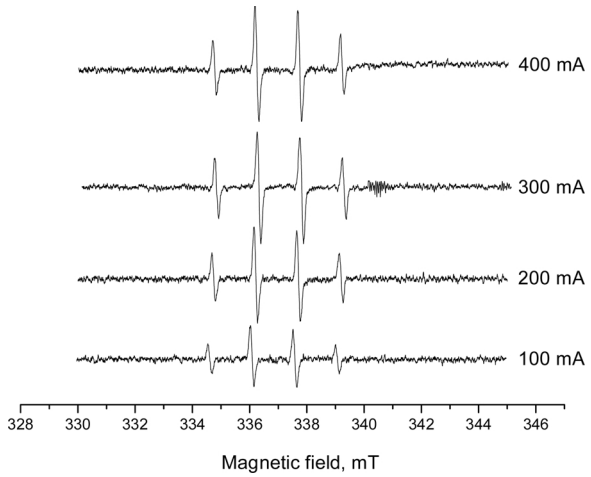

Fig. 12. DMPO spin trapping EPR spectra over the double perovskite in EF system at various current intensity.

the bulk via Eq. (19) and its destruction by H_2O_2 (Eq. (20)), $\equiv Fe^{2+}$ and $\equiv Cu^{+}$ (Eqs. (21) and (22), respectively) can also take place [45].

$$2BDD(^{\cdot}OH) \rightarrow 2BDD + O_2 + 2H^{+} + 2e^{-} \quad (17)$$

$$2BDD(^{\cdot}OH) \rightarrow 2BDD + H_2O_2 \quad (18)$$

$$2^{\cdot}OH \rightarrow H_2O_2 \quad (19)$$

$$H_2O_2 + {}^{\cdot}OH \rightarrow HO_2^{\cdot} + H_2O \quad (20)$$

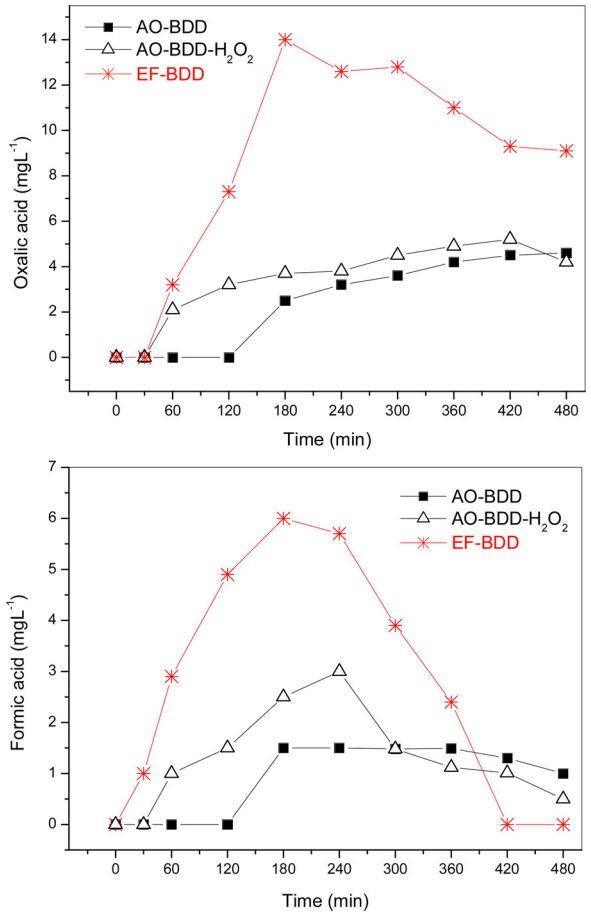

Fig. 13. Time-course of the concentration of oxalic and formic acids detected during the treatments shown in Fig. 7.

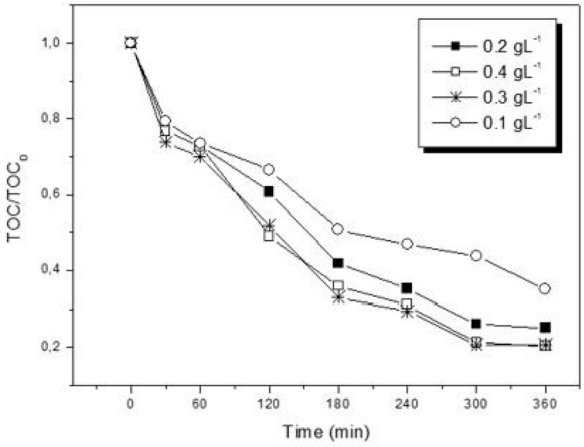

Catalyst loading (gL^{-1})	K (min^{-1})	R^2
0.1	0.00291	0.989
0.2	0.00380	0.990
0.3	0.00500	0.993
0.4	0.00506	0.994

Fig. 14. Effect of the catalyst loading on the cotinine mineralization by electro-Fenton process. Experimental conditions: $[Na_2SO_4]$ = 0.05 M, pH = 3.0, I = 200 mA, working volume of 500 mL, $[cotinine]_0$ = 50 mg L^{-1}.

$$\equiv Fe^{2+} + {}^{\cdot}OH \rightarrow \equiv Fe^{3+} + OH^{-} \quad (21)$$

$$\equiv Cu^{+} + {}^{\cdot}OH \rightarrow \equiv Cu^{2+} + OH^{-} \quad (22)$$

The MCE values have been estimated from Eq. (14). Obviously, the current efficiency for the applied processes decreased when the current intensity increased. This behavior is typical of EAOPs and it's usually related to the scavenging of produced radicals by the wasting reactions discussed above.

Moreover, the MCE values underwent a significant decrease with prolonging electrolysis. This general trend can be related to the progressive decay in organic charge of the medium along with the formation of more recalcitrant products.

The aforementioned findings corroborate the viability of H-EF-BDD for the cotinine remediation. For industrial scale low current values are more favorable since they yield more economic process with lower EC_{TOC}, although longer times are needed for reaching total mineralization.

Ion exclusion chromatograms of electrolyzed solutions at 8 mAcm^{-2} revealed the major generation of 2 carboxylic acids: oxalic and formic acids. These compounds are the ultimate acids since they would be directly mineralized to CO_2 and H_2O. Oxamic acid which is usually expected to be formed from the destruction of N-intermediates with a NH_2-group, has not been identified in this study. Fig. 13 highlights that formic acid is only accumulated to almost 1.5 and 3 mg L^{-1} after 4 h before to be slowly removed by BDD ($^{\cdot}OH$) in AO and AO-H_2O_2, whereas in Hetero EF-BDD it is much more largely accumulated up to 6 mg L^{-1} after 3 h, disappearing after 420 min of electrolysis. The higher concentration achieved by formic acid in the EF process could be related to the quicker degradation of cotinine and its organic intermediates. The same figure depicts that oxalic acid is poorly accumulated by AO and AO-H_2O_2 (< 5 mg L^{-1}), attaining a concentration of 14 mg L^{-1} at 180 min of EF, which only falls to 9.1 mg L^{-1} at the end of electrolysis. Acetic acid and succinic acid with a very low extent have also been detected during the cotinine electrolysis.

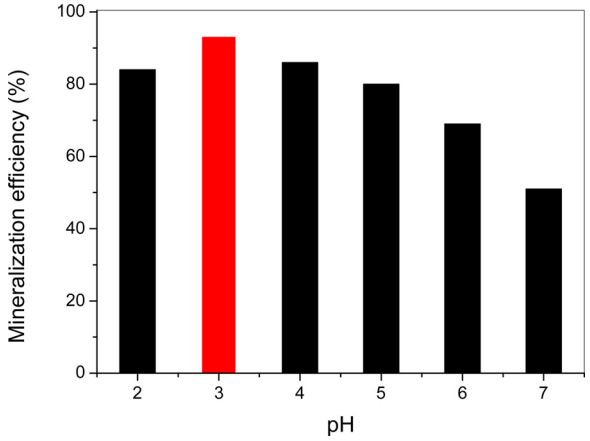

Fig. 15. Effect of the initial pH on the cotinine mineralization by electro-Fenton process. Experimental conditions: $[Na_2SO_4]$ = 0.05 M, I = 200 mA, working volume of 500 mL, $[cotinine]_0$ = 50 mg L^{-1}.

4.3. Effect of the catalyst dosage

The efficiency of the heterogeneous EF process is also governed by the amount of the heterogeneous catalyst and the available active sites on its surface. Fig. 14 illustrates the cotinine mineralization efficacy at a constant current of 200 mA and for various Sr_2FeCuO_6 ranging from 0.1 to 0.4 g L^{-1}. Note that under all conditions, mineralization kinetics well fitted a pseudo-first-order reaction and the kinetic analysis of curve 14 are summarized in Fig. 14. Noticeably, the rise in catalyst loading from 0.1 to 0.3 g L^{-1} was accompanied by a rise in the mineralization rate due to the availability of more active sites for the activation of the electro-generated H_2O_2. However, non-significant enhancement was observed when the solid catalyst concentration was increased from 0.3 to 0.4 g L^{-1}. This could be explained by the scavenging effect of iron and cuprous sites on the generated $^{\cdot}OH$ (Eqs. (21) and (22)).

4.4. Effect of the initial pH

The solution pH is an important parameter for controlling the performance of the electro-Fenton process. It is well documented in the literature that the presence of protons favors the electro-generation of hydrogen peroxide through the two-electron reduction of oxygen given by Eq. (3).

In this study, the effect of initial pH was examined in the range 2–7. Fig. 15 shows that after 8 h of treatment, the mineralization removal was 84, 93, 86, 80, 69 and 51% for the values of pH 2, 3, 4, 5, 6 and 7 respectively. Since the highest efficiency (93%) was observed at pH of 3, it was chosen as the optimum pH. The efficiency decreases with increasing the pH value due to the fact that a low pH is more favorable for the production of hydrogen peroxide. Moreover, it is well known that the stability of hydrogen peroxide is affected by the pH. Above pH 4, H_2O_2 become unstable and begins to decompose easily to form water and oxygen according to the following reaction:

$$2H_2O_2 \rightarrow 2H_2O + O_2 \quad (23)$$

The slight decrease in the process efficiency observed at pH 2 could be ascribed to the formation of oxonium ions ($H_3O_2^+$) which could limit the formation of hydroxyl radicals.

$$\text{For pH} < 3\text{: } H_2O_2 + H^+ \rightarrow H_3O_2^+ \quad (24)$$

4.5. Identification of Cotinine by-products during the EF process

To elucidate the cotinine oxidation pathway, intermediates formed during the EF-perovskite treatment were identified by GC–MS analysis. Since organics are mainly attacked by hydroxyls radicals, same oxidation intermediates are expected in all the tested EAOPS. Considering the quicker cotinine oxidation under higher current values, trial was performed at 4 mA cm^{-2} in order to avoid the fast degradation of the metabolites. In addition, to ensure their accumulation and detection, a high cotinine concentration was used (300 mg L^{-1}). The identification was based on the mass fragmentation values and by comparing the mass spectra to a database. Seven intermediates were detected, but only four of them were identified. The recognized metabolites were N'-Hydroxymethylnorcotinine (tr = 27.35 min), norcotinine (tr = 23.92 min), 4-oxo-4-(3-pyridyl) butanoic acid (tr = 5.07 min) and 4-(3-Pyridyl)-3-butenoic Acid (tr = 20.779 min). Table 2 summarizes the characteristics of these intermediates and Fig. S1 shows their mass spectra. The mass spectra of cotinine and the non-identified compounds are also illustrated in Fig. S1. According to the reactivity of hydroxyl radicals, hydroxylation reaction occurred during the first stage of oxidation, which leads to the formation of the major intermediate N'-Hydroxymethyl norcotinine, in which electrophilic addition of $^{\cdot}OH$ takes place. Further radical attack at the amino group of the molecule leads to the formation of norcotinine through a demethylation reaction. Subsequent leakage of the pyrrolidine nucleus and the degradation of its lateral group, yielded to the formation of 4-oxo-4-(3-pyridyl) butanoic acid and 4-(3-Pyridyl)-3-butenoic Acid. Progressive cleavage leads to the apparition of compounds with lower molecular weight. Ultimate ring-opening of these aromatic intermediates leads to formation of short-chain carboxylic acids, which are generally reported as the end-products before total mineralization to CO_2, water and inorganic nitrogen. The suggested mechanism (Fig. 16) is in good agreement with that proposed by J. Hukkanen [2] for the pathways of nicotine metabolism, in which several of the identified intermediates coincided with the ones we found (Table 2).

4.6. Catalyst recyclability

Finally, to assess the economic viability of the developed magnetic catalyst, its reusability has been tested. Unexpectedly, as illustrated in Table 3, a rise in the mineralization rate was observed in the second and third cycle which could be explained by the formation of new actives sites on the catalyst surface after contact with the aqueous medium. Based on the XPS results, we can conclude that the higher catalytic activity observed after the first and second catalytic cycle is due to the increase in the oxygen extent on the double perovskite surface. Similar behavior was reported by Taran et al. [46] who studied the wet peroxide oxidation of phenol using the single perovskite catalyst $LaFeO_3$. We suggest that the formation of hydroxyl groups and water molecules on the surface of spent catalysts may be the reason of the enhancement in the catalytic yield since they would be involved directly in the mechanism of oxidation.

5. Conclusion

Single phase Sr_2FeCuO_6 double perovskite was synthesized by citrate gel method and applied as heterogeneous Fenton catalyst for the electrochemical oxidation of cotinine as a compound of emergent concern. The mineralization of 500 mL of 50 mg L^{-1} cotinine at pH 3.0 were studied by anodic oxidation and electro-Fenton (EF) process. Trials were performed in a one compartment cell equipped with a boron-doped diamond (BDD) anode and a carbon felt cathode. The viability of the EF process to mineralize a cotinine solutions of pH 3.0 has been demonstrated. The mineralization of cotinine solutions were much faster for heterogeneous EF under comparable conditions. The increase in the current intensity was accompanied by a rise in the mineralization efficiency through the concomitant production of more oxidizing agents, but with gradual decay in MCE by the greater acceleration of parasitic reactions. The EPR results indicate that the hydroxyl radicals ($^{\cdot}OH$) were the dominant reactive oxygen species generated

Table 2
Chemical structure, retention time and main mass fragmentation values of the identified cotinine intermediates formed during the EF process.

Identification number	Compound	Formula	Structure	Molecular mass ($gmol^{-1}$)		Tr (min)	Main mass fragmentation value (m/z)
I	N-Hydroxymethyl norcotinine	$C_{10}H_{12}N_2O_2$	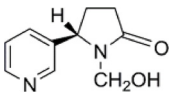	192	27.35		161.1/133/ 105/79
II	Norcotinine	$C_9H_{10}N_2O$	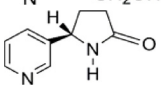	162	23.92		134/105/77
III	4-oxo-4-(3-pyridyl) butanoic acid	$C_9H_9NO_3$	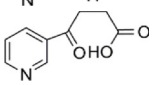	179	5.072		149/ 132.8/119
IV	4-(3-Pyridyl)-3-butenoic Acid	$C_9H_9NO_2$	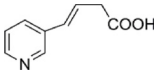	163.17	20.779		162/118 /105 /77

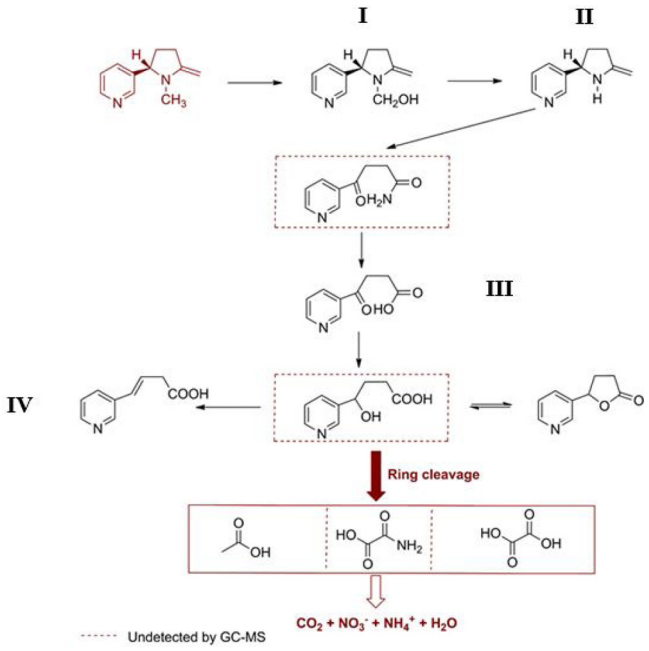

Fig. 16. Proposed pathway of cotinine mineralization by the heterogeneous Sr_2FeCuO_6 electro-Fenton process.

Table 3
$Sr_2FeCuO6$ reusability. Experimental conditions: $[Na_2SO_4]$ = 0.05 M, pH = 3.0, I = 200 mA, working volume of 500 mL, catalyst loading = 0.3 g L^{-1}, $[cotinine]_0$ = 50 mg L^{-1}.

Cycle	Reaction Time, hours	TOC removal (%)	K (min^{-1})
1	6	82.29	0.00500
2	6	87.41	0.00683
3	6	84.67	0.00597

during the catalytic treatment of cotinine under the heterogeneous electro-Fenton system. Organics were removed by hydroxyl radical (˙OH) formed: (i) at the BDD anode from water oxidation, and (ii) from Fenton's reaction between added catalyst and generated H_2O_2 at the cathode. Moreover, the synergistic effect of cuprous ions was pointed out, stimulating further investigation on the use of various transition metals as co-catalysts for improving the performance of heterogeneous EF/perovskite process. At pH 3, TOC removal followed the order of Sr_2FeCuO_6-EF- BDD > $SrFeO_6$-EF- BDD > $SrCuO_6$-EF- BDD > AO-H_2O_2-BDD > AO-BDD.

The initial N atoms of the target molecule were pre-eminently accumulated as NO_3^- ion. A plausible general reaction sequence for cotinine mineralization involving all oxidation products detected was proposed. Furthermore, the Sr_2FeCuO_6 exhibited excellent long-term stability in the heterogeneous EF process. These results suggested that the novel magnetic double perovskite material would be a promising candidate for practical wastewater treatment.

Appendix A. Supplementary data

Supplementary material related to this article can be found, in the online version, at doi:https://doi.org/10.1016/j.apcatb.2018.09.002.

References

[1] V. Rakic, L. Damjanovic, V. Rac, D. Stosic, V. Dondur, A. Auroux, Water Res. 44 (2010) 2047–2057.
[2] J. Hakkinen, P. Jacob, N.L. Benowitz, Pharmacol. Rev. 57 (2005) 79–115.
[3] J.R. Masoner, D.W. Kolpin, E.T. Furlong, I.M. Cozzarelli, J.L. Gray, E.A. Schwab, Environ. Sci: Process. Impacts 16 (2014) 2335–2354.
[4] J. Schwarzbauer, S. Heim, S. Brinker, R. Littke, Water Res. 36 (2002) 2275–2287.
[5] W.J. Andrews, J.R. Masoner, I.M. Cozzarelli, Groundwater Monit. Requirements 32 (2012) 120–130.
[6] P.M. Buszka, D.J. Yeskis, D.W. Kolpin, E.T. Furlong, S.D. Zaugg, M.T. Meyer, Waste-indicator and pharmaceutical compounds in landfill-leachate-affected ground water near Elkhart, Indiana, 2000–2002, Bull. Environ. Contam. Toxicol. 82 (2009) 653–659.
[7] S. Bastianini, V. Lo Martire, A. Silvani, G. Zoccoli, C. Berteotti, H. Lagercrantz, A. Amer, G. Cohen, Acta Paediatr. 107 (2018) (2018) 638–646, https://doi.org/10.1111/apa.14181.
[8] M.A. Oturan, J.J. Aaron, Environ. Sci. Technol. 44 (2014) (2014) 2577–2641.
[9] E. Brillas, C.A. Martínez-Huitle, Appl. Catal. B 166–167 (2015) 603–643.
[10] I. Sirés, E. Brillas, M.A. Oturan, M.A. Rodrigo, M. Panizza, Environ. Sci. Pollut. Res. Int. 21 (2014) 8336–8367.
[11] F.C. Moreira, R.A.R. Boaventura, E. Brillas, V.J.P. Vilar, Appl. Catal. B: Environ. 202 (2017) 217–261.
[12] A. Özcan, Y. Sahin, M.A. Oturan, Water Res. 47 (2013) 1470–1479.
[13] B. Balci, N. Oturan, R. Cherrier, M.A. Oturan, Water Res. 43 (2009) 1924–1934.
[14] S. Garcia-Segura, J.A. Garrido, R.M. Rodrıguez, P.L. Cabot, F. Centellas, C. Arias, E. Brillas, Water Res. 46 (2012) 2067–2076.
[15] E. Mousset, N. Oturan, E.D. Van Hullebusch, G. Guibaud, G. Esposito, M.A. Oturan, Appl. Catal. B 160–161 (2014) 666–675.
[16] M. Panizza, G. Cerisola, Chem. Rev. 109 (2009) 6541–6569.
[17] H. Zhang, C. Fei, D. Zhang, F. Tang, J. Hazard. Mater. 145 (2007) 227–232.
[18] E. Mousset, L. Frunzo, G. Esposito, E.D. Van Hullebusch, N. Oturan, M.A. Oturan, Appl. Catal. B-Environ. 180 (2016) 189–198.
[19] M. Pimentel, N. Oturan, M. Dezotti, M.A. Oturan, Appl. Catal. B: Environ. 83 (2008) 140–149.
[20] A. Özcan, A.A. Özcana, Y. Demirci, E. Sener, Appl. Catal. B: Environ. 200 (2017) 361–371.
[21] Q. Peng, H. Zhao, L. Qian, Y. Wang, G. Zhao, Appl. Catal. B: Environ. 174–175 (2015) 157–166.
[22] N. Barhoumi, N. Oturan, S. Ammar, M.A. Oturan, E. Brillas, Environ. Chem. Lett. 15 (2017) 689–693.
[23] S. Ammar, M.A. Oturan, L. Labiadh, A. Guersalli, R. Abdelhedi, N. Oturan, E. Brillas, Water Res. 74 (2015) 77–87.
[24] S.B. Hammouda, F. Zhao, Z. Safaei, V. Srivastava, D.L. Ramasamy, S. Iftekhar,

S. Kalliola, M. Sillanpää, Appl. Catal. B: Environ. 215 (2017) 60–73.
[25] S.B. Hammouda, F. Zhao, Z. Safaei, I. Babu, D.L. Ramasamy, M. Sillanpää, Appl. Catal. B: Environ. 218 (2017) 119–136.
[26] H. Lin, X.X. Shi, X.M. Chen, J. Alloys. Compd 709 (2017) 772–778.
[27] M. Saxena, K. Tanwar, T. Maiti, Scr. Mater. 130 (2017) 205–209.
[28] Y. Mao, J. Parsons, J.S. McCloy, Nanoscale 5 (2013) 4720–4728.
[29] D.D. Sarma, E.V. Sampathkumaran, S. Ray, R. Nagarajan, S. Majumdar, A. Kumar, G. Nalini, T.G. Row, Solid State Commun. 114 (2000) 465–468.
[30] Y.Q. Lin, X.M. Chen, X.Q. Liu, Solid State Commun. 149 (2009) 784–787.
[31] Y.Q. Lin, X.M. Chen, J. Am. Ceram. Soc. 94 (2011) 782–787.
[32] J.L. Sotelo, G. Ovejero, F. Martınez, J.A. Melero, A. Milieni, Appl. Catal. B: Environ. 47 (2004) 281–294.
[33] A. Ozcan, Y. Sahin, A.S. Koparal, M.A. Oturan, Appl. Catal. B-Environ. 89 (2009) 620–626.
[34] W.T. Chen, M. Mizumaki, T. Saitoa, Y. Shimakawa, Dalton Trans. 42 (2013) 10116–10118.
[35] N. Russo, D. Mescia, D. Fino, G. Saracco, V. Specchia, Ind. Eng. Chem. Res. 46 (2007) 4226–4231.
[36] J. Chen, Z. He, G. Li, T. An, H. Shi, Y. Li, Appl. Catal. B: Environ 209 (2017) 146–154.
[37] P.N. Lekshmi, M. Vasundhara, M.R. Varma, K.G. Suresh, M. Valant, Phys. B: Condens. Matter 448 (2014) 285–289.
[38] F. Jin, Y. Shen, R. Wang, T. He, J. Power Sources 234 (2013) 244–251.
[39] L. Zhang, Q. Zhou, Q. He, T. He, J. Power Sources 195 (2010) 6356–6366.
[40] H. Falcón, J.A. Barbero, G. Araujo, M.T. Casais, M.J. Martınez-Lope, J.A. Alonso, J.L.G. Fierro, Appl. Catal. B: Environ. 53 (2004) 37–45.
[41] J.M. Fontmorin, R.C.B. Castillo, W.Z. Tang, M. Sillanpää, Water Res. 99 (2016) 24–32.
[42] X. Hu, B. Liu, Y. Deng, H. Chen, S. Luo, C. Sun, P. Yang, S. Yang, Appl. Catal. B: Environ. 107 (2011) 274–283.
[43] S. Garcia-Segura, E. Mostafa, H. Baltruschat, Appl. Catal. B 207 (2017) 376–384.
[44] E.B. Cavalcanti, S. Garcia-Segura, F. Centellas, E. Brillas, Water Res. 47 (2013) 1803–1815.
[45] Y. Wang, H. Zhao, S. Chai, Y. Wang, G. Zhao, D. Li, Chem. Eng. J. 223 (2013) 524–535.
[46] O.P. Taran, A.B. Ayusheev, O.L. Ogorodnikova, I.P. Prosvirin, L.A. Isupova, V.N. Parmon, Appl. Catal. B: Environ. 180 (2016) (2016) 86–93.